Submitted to
Physics Letters
October 1974

FERMILAB-PUB-74-160-E

# TOPOLOGICAL AND LEADING PARTICLE CROSS SECTIONS FOR 147 GeV/c $\pi^-$ - p INTERACTIONS*

D. G. Fong, M. Heller, A. M. Shapiro, and M. Widgoff

Brown University
Providence, Rhode Island 02912

D. Bogert and M. Johnson

FERMILAB
Batavia, Illinois 60510

C. -Y. Chien, P. Lucas, A. Pevsner, and R. A. Zdanis

Johns Hopkins University
Baltimore, Maryland 21218

R. A. Burnstein, C. Fu, D. V. Petersen, R. M. Robertson, and H. A. Rubin

Illinois Institute of Technology
Chicago, Illinois 60616

R. D. Sard, A. E. Snyder, and J. Tortora

University of Illinois
Urbana, Illinois 61801

E. D. Alyea, Jr.

Indiana University
Bloomington, Indiana 47401

F. Bruyant[+], J. Grunhaus[++], E. Hafen, R. I. Hulsizer, U. Karshon[+++], V. Kistiakowsky, A. Levy[++], A. Napier, I. A. Pless, P. Trepagnier, J. Wolfson, and R. K. Yamamoto

Massachusetts Institute of Technology
Cambridge, Massachusetts 02139

H. O. Cohn

Oak Ridge National Laboratory
Oak Ridge, Tennessee 37830

T. C. Ou, R. J. Plano, and T. L. Watts

Rutgers University
New Brunswick, New Jersey 08903

E. B. Brucker, E. L. Koller, P. Stamer, and S. Taylor

Stevens Institute of Technology
Hoboken, New Jersey 07030

W. M. Bugg, G. T. Condo, and E. L. Hart

University of Tennessee
Knoxville, Tennessee 37916

W. Barletta[**], D. Dauwe[***], M. Kenton, H. Kraybill, D. Ljung, T. Ludlam, and H. Taft

Yale University
New Haven, Connecticut 06520

Results are reported based on a study of $\pi^-p$ interactions at 147 GeV/c in the FERMILAB 30-inch Proportional Wire Hybrid Bubble Chamber System. We have measured the topological cross sections and separated two-prong elastic and inelastic channels. In addition, we have extracted leading particle cross sections using the increased momentum resolution of the downstream proportional wire chambers. We have compared our results with other experiments and predictions of a simple fragmentation hypothesis.

* This work supported in part by the United States Atomic Energy Commission and the United States National Science Foundation.

+ Permanent address, CERN, Geneva, Switzerland.

++ On leave of absence, Tel-Aviv University, Israel.

+++ On leave of absence, The Weizmann Institute of Science, Israel.

** Present address, Lawrence Livermore Laboratory, California

*** Present address, University of Illinois, Illinois

# Topological and Leading Particle Cross Sections for 147 GeV/c $\pi^-$-p Interactions

Introduction: The results presented in this paper are the first obtained in the 30-inch Proportional Wire Hybrid Bubble Chamber System at FERMILAB. An exposure of 100,000 pictures, with an average of five beam tracks per frame, was made in a beam of 147 GeV/c $\pi^-$ mesons [1]. The exposure was taken during March 1974, and most of the analysis presented here is based on about 30% of the film. The cross sections for the various charged particle multiplicities are based on about 40% of the film. An upstream proportional wire system, plus a Čerenkov counter, tagged $\pi^-$, $\bar{p}$ and $K^-$ in the incident beam, while the downstream proportional wire system furnished accurate momentum measurements of the fast forward particles. A unique feature of this hybrid system is that no trigger is required for event selection. Hence, all data associated with each incident beam particle are automatically stored on magnetic tape and are available for later processing. Utilizing the improved (over bare bubble chamber techniques) momentum resolution on fast outgoing particles, we report here on the leading particle cross sections.

Experimental details: The Proportional Wire Hybrid Bubble Chamber System at FERMILAB consists of the 30-inch bubble chamber immersed in a 26 kilogauss field with a series of proportional wire chambers (PWC) both upstream and downstream. A sketch of an elevation view of the system is shown in Figure 1.

The PWC configuration consists of 2,900 wires, each of which is connected to a 16 bit storage register. The effective dead time of the electronic system is 120 nanoseconds, so that with a standard particle spill of 100 microseconds and less than 10 incident beam particles per spill, the pile-up losses are negligible. The history of each particle incident on the bubble chamber is recorded in the storage registers and transferred to computer memory between bubble chamber expansions. We emphasize that no triggering or event preselection is performed. Measurements

of the noninteracting beam tracks,with and without magnetic field, are used to connect the bubble chamber coordinate system to the proportional wire coordinate system to an accuracy of better than 50 microns in space. With the additional magnetic path due to the fringe field of the bubble chamber and the long lever arm of the PWC system, particle momentum measurements are made with an error of $\Delta p/p \sim .06\ p\%$ with p measured in units of GeV/c. The shaded areas in Figures 2(a), (b), and (c) show the fraction of $\pi^-$ tracks (for 2, 4, and 6-prong events) actually captured in the downstream system. The upstream system has an angular resolution of .004 milliradians and when used in conjunction with the Čerenkov counter, it allows tagging of $\pi^-$, $K^-$, $\bar{p}$ in the incident beam.

The bubble chamber film was first predigitized on scanning tables and then measured with PEPR. These measurements were processed through an automatic match-geometry program called GEOMAT. The PWC information, which is stored on magnetic tape, is processed by a reconstruction program called the Proportional Wire Geometry Program (PWGP) which utilizes the vertex of the event as determined by GEOMAT to form track trajectories from the wire data. The final track four vectors are calculated by a program called Track Organizer which correlates all the available information from GEOMAT and PWGP. Since these are new programs, every event was examined at the scan table by physicists to compare the output of Track Organizer with the film image.

Elastic Scattering: The PWC system provides a sensitive technique for separating elastic from inelastic events in the 2-prong sample. A typical low-t, 2-prong event traversing the system is sketched in Figure 1. The angle of the incident beam track is measured to an accuracy limited only by multiple scattering ( $\sim .05$ mr ) which, coupled with the well determined beam momentum, gives an uncertainty in the transverse momentum of the beam of less than 10 MeV/c. The recoil proton is measured in the bubble chamber in the usual way, with the momentum determined to a few MeV/c. Thus, we can make an accurate prediction of the trajectory of the

outgoing fast pion for the hypothesis that the event was elastic. This prediction is then compared with the observed trajectory in the downstream counters. To select elastic events we compare the predicted and observed positions in the farthest downstream chamber (chamber G) by forming the quantity

$$R^2 = (Y_{pred} - Y_{obs})^2 + (Z_{pred} - Z_{obs})^2$$

where $(Y_{pred}, Z_{pred})$ and $(Y_{obs}, Z_{obs})$ are, respectively, the predicted and observed positions at chamber G in the plane transverse to the beam line. The spatial resolution of the downstream PWC system is about 0.3 mm. The uncertainty of the predicted position, determined by the accuracy with which the recoil proton can be reconstructed, is about 0.5 mm.

The distribution in $R^2$ for the 2-prong sample is shown in Figure 3a in which the elastic signal is clearly seen. The shape of this signal is in excellent agreement with the expected result as obtained from Monte Carlo simulations. We accept as elastic all 2-prong events with $R^2 < 10\ mm^2$. This technique is roughly equivalent to a 3 constraint fit and is sensitive to a transverse momentum imbalance of 50 MeV/c or greater. As a result of Monte Carlo simulation and of simulating 2-prong events coming from quasi-elastic 4-prongs (discarding 2 slow pions), we estimate an upper limit of 5% inelastic contamination in our elastic sample. Further, we estimate that the inelastic 2-prong sample thus obtained contains less than 7% contamination from elastic events. Thus, the external detectors provide clear separation of elastic and inelastic 2-prongs. In calculating cross sections, a correction is made for fast outgoing tracks which scatter in the exit window of the bubble chamber and hence are lost to the downstream system. This is a 6% correction to the elastic cross section and a 3% correction for the inelastic cross section.

After accounting for all corrections, including that for a systematic scanning bias against low-t events (elastic: 17%, inelastic: 6%), we find the elastic and inelastic cross sections to be $3.08 \pm 0.21$ mb and $2.07 \pm 0.17$ mb respectively. The

elastic differential cross section is shown in Fig. 3b. The slope parameter, assuming a form $\frac{d\sigma}{dt} \sim e^{bt}$, was found by fitting in the range $0.04 < -t < 0.4$ $(GeV/c)^2$. The result obtained is $b = 8.5 \pm 1.5$ $(GeV/c)^{-2}$.

Topological Cross Sections: Topological cross sections are given in Table 1, together with the total and elastic cross sections, and are plotted in Figure 4. These values of the cross sections are based on a sample corresponding to $3.24 \pm 0.04$ $\mu$barn/event. This number has been corrected for 1.3% muon contamination in the beam. For the density of liquid hydrogen, we used the value $0.0627 \pm 0.0005$ gm/cm$^3$ obtained by Bogert et al. [2]

The following corrections were made to obtain the topological cross sections from the scanning data: (1) scanning efficiency as a function of topology; (2) 2-prong events lost because of low momentum transfer; (3) Dalitz pairs not identified in scanning; (4) close secondary interactions and short stubs: the fifty events with an odd number of prongs can be accounted for by these two causes and were reassigned to even topology categories accordingly; (5) close $V^0$ decays and electron pairs: any error due to this appeared to be negligible.

Some moments of the multiplicity distribution are given in Table II, together with the corresponding results found at 50[3], 100[4], and 205[2] GeV/c. Our measured value of the mean multiplicity $\langle n_{ch} \rangle$ is $7.34 \pm 0.10$ at 147 GeV/c. We have fit the data for $\langle n_{ch} \rangle$ at the four momenta to the formula: $\langle n_{ch} \rangle = a + b \ln s/s_0$ with $s_0 = 1$ GeV$^2$. We find:

$$a = -1.2 \pm 0.3$$

$$b = 1.54 \pm 0.07$$

with a chi-square of 2.0 for two degrees of freedom or a 35% confidence level. This is in good agreement with the calculation in reference (4).

Leading Particle Cross Sections: In Figure 2, we display the Feynman x distributions for the $\pi^-$ mesons and for protons in the 2, 4, and 6-prong samples. In

order to calculate a leading particle cross section for the 2-prong sample, we must separate the elastic events from the inelastic events on an event by event basis. The method of this separation was discussed above and the results are shown in the inserts in Figures 2a and 2d.

The elastic peak in Figure 2a is an indication of our resolution function at $x = 1$. Hence, we can use this experimentally determined resolution function to unfold the leading pion cross sections. Clear leading pion peaks are seen in the 2-prong inelastic and 4-prong samples while only an excess over zero is evident in the 6-prong sample. The leading pion cross sections given in Table III were obtained by measuring the areas under these peaks. For the 2-prong inelastic sample and the 4-prong sample we are able to determine the cross sections; for the 6-prong sample the measurement can be considered an upper limit. Small corrections have been made to all the data for low-t events and interactions in the bubble chamber exit window. We find no evidence for a leading particle effect in any higher multiplicity sample. We have identified protons by measuring the ionization of slow (less than 1.0 GeV/c ) positive tracks. We have determined the leading proton cross sections by selecting protons with x less than -0.9.

Factorization: We can use the above results to test whether $\pi p$ and $pp$ elastic scattering and the leading particle reactions are mediated by the same factorizable exchange, for which the most likely candidate is the Pomeron. The hypothesis underlying the test implies the following relation:

$$\frac{\sigma\,(pp \to pp)}{\sigma\,(\pi^- p \to \pi^- p)} = \frac{\sigma\,(pp \to \text{leading proton})}{\sigma\,(\pi^- p \to \text{leading pion})}$$

From the pp data at 205 GeV/c[5] and the $\pi^-$ - p data in this experiment, we can calculate the two ratios. We find the ratio of the elastic scattering cross sections to be $2.25 \pm 0.20$, while we find the ratio for the right hand side of the relation to

be 1.4 ± 0.4 for 2-prong events and 1.3 ± 0.3 for 4-prong events. The latter measurement may indicate ~ 3 standard deviation violation of this type of factorization.

We can also use our data to calculate the extent to which the low multiplicity cross sections in this experiment can be accounted for by a factorizable exchange mediating elastic scattering plus low mass diffractive excitation of the target, the projectile, or both. If the cross section is factorizable, as above, into either target or projectile or both fragmenting into low mass clusters, then the topological cross sections $\sigma^N(t)$ for producing N charged particles, at fixed t, can be expressed as:

$$\sigma^N(t) = \sigma^N_{L\pi}(t) + \sigma^N_{Lp}(t) + \frac{1}{\sigma_{el}(t)} \sum_{j=0}^{\frac{N-2}{2}} \sigma_{L\pi}^{N-2j}(t) \cdot \sigma_{Lp}^{2j+2}(t)$$

In the above $\sigma_{el}(t)$ is the elastic cross section, while $\sigma^N_{L\pi}(t)$ is the leading pion cross section and $\sigma^N_{Lp}(t)$ is the leading proton cross section for the N charged prong multiplicity (note that N is a non zero even integer).

Using this relation we have calculated the total diffractive contribution of the 2, 4, and 6-prong events, using the leading particle cross sections given in Table III. We have numerically integrated the right hand side by suitably binning our data. Our results for the right hand side are as follows:

1. For the inelastic 2-prong cross section, we calculate 1.62 ± 0.24 mb. This is only 1.5 standard deviations smaller than the measured topological cross section of 2.07 ± 0.17 mb listed in Table III.

2. For the 4-prong cross section, we calculate 2.27 ± 0.22 mb, which is almost a factor two smaller than the 4.10 ± 0.14 mb listed in Table III.

3. For the 6-prong cross section, we calculate 0.99 ± 0.18 mb, which is almost a factor five smaller than the 4.61 ± 0.14 mb listed in Table III. From these calculations, we conclude that a factorizable exchange resulting in low mass

excitation of the pion, the proton, or both, is unlikely to be responsible for more than half of all the 2, 4, and 6-prong cross sections.

Conclusions: We have studied $\pi^-$ - p interactions at 147 GeV/c incident momentum using a PWC Hybrid Bubble Chamber System. We report on the first measurements with this system.

We have isolated and measured the elastic $\pi^-$p cross section and we find this cross section to be $\sigma_{el} = 3.08 \pm 0.21$ mb. The elastic slope was fitted between $.04 < -t < .4$ $(GeV/c)^{-2}$ to the form $\sigma_{el} \sim e^{bt}$. We find $b = 8.5 \pm 1.5$ $(GeV/c)^{-2}$. Using our knowledge of the elastic channel, we can identify the 2-prong inelastic channel.

We have measured the x distribution of the $\pi^-$ mesons and protons for the 2, 4, and 6-prong topologies. Using this data we have determined the leading particle cross sections and find the ratio of the leading proton to the leading pion to be roughly one for the 2, 4, and 6 charged prong topologies.

We have compared our results with the pp measurements at 205 GeV/c and find that while the 2-prong data is consistent with a factorizable Pomeron exchange model, the 4-prong comparison might indicate a 3 standard deviation from this model. In addition, the measurements from this experiment indicate that the 4 and 6-prong final states are not produced solely by a factorizable fragmentation of the beam and target into low mass enhancements or clusters, but that approximately half or more of the cross section is due to some other process.

Acknowledgments: We thank the personnel of the FERMILAB Neutrino Section and 30-inch bubble chamber facility whose skills and efforts made this experiment possible. We also thank our data reduction personnel for their efficient scanning and measuring of the film. In addition, we wish to acknowledge enlightening discussions with F. E. Low and R. Slansky.

## REFERENCES

(1) The PWC Hybrid System has been used to measure the average incident beam momentum: $p_{\pi} = 146.75 \pm 0.76$ GeV/c, with a dispersion of 0.65 GeV/c. Internal Report PHSC Newsnote No. 30 - Brief Summary of Survey Results for Exp. 154 - 9 August 1974, unpublished.

(2) Bogert et al. Phys. Rev. Letters 31, (1973) 1271.

(3) G. A. Akopdjanov et al. Nucl. Phys. B. 75 (1974) 401.

(4) E. L. Berger et al. CERN/D. Nucl. Phys. B. 77 (1974) 365.

(5) S. J. Barish et al. Phys. Rev. Letters 31, (1973) 1080 and Phys. Rev. D. 9, (1974) 1171.

# TABLE CAPTIONS

TABLE I

Topological Cross Sections

TABLE II

Some moments of the multiplicity distribution. $f_2 = \langle n(n-1) \rangle \div \langle n \rangle^2$.

$D = (\langle n^2 \rangle - \langle n \rangle^2)^{\frac{1}{2}}$. a - see reference (3).

b - see reference (4). c - see reference (2).

TABLE III

Leading particle and total inelastic cross sections for 2, 4, and 6-prong events in millibarns.

FIGURE CAPTIONS

Figure 1: Elevation view of the 30" PWC Hybrid Bubble Chamber System. Chambers A, B, and C each contain 3 planes of dimensions 4" x 4" active area placed $120^0$ apart in angle. PWC I is used to improve the momentum resolution of the incident beam. The spacing between sense wires is 2 mm with a total of 150 wires per chamber. Chambers D, E, F, and G are composed of planes 12" x 12" with 2 mm sense wire spacing. There is a total of sixteen planes in these chambers, 4 in D, 3 in E, 4 in F, and 5 in G. The Scintillator counter telescope (SCI and SCII) forms a 5 nanosecond gate which is used to strobe the PWC data into the 16-Bit storage registers which are connected to each sense wire. The dead time of this operation is 120 nanoseconds, hence pile-up losses are small.

Figure 2: $\pi^-$ meson and proton x distribution. a) - c) give the $\pi^-$ meson data while d) - f) give the proton data. The shaded areas are those tracks for which the downstream PWC equipment determined the momentum.

a) Two prong $\pi^-$ sample. The insert is the inelastic sample. See text for the details of this separation.

b) Four prong $\pi^-$ data

c) Six prong $\pi^-$ data

d) Two prong proton sample. The insert is the inelastic sample. See text for details of separation.

e) Four prong proton sample

f) Six prong proton sample

Figure 3: Elastic scattering data.

a) The experimental distribution in $R^2$. See text for details.

b) $\frac{d\sigma}{dt}$ for $\pi^-$ p elastic scattering. The solid curve is a fit to the relation

$$\sigma(t) \sim e^{bt}, \text{ with } b = 8.5 \pm 1.5 \text{ (GeV/c)}^{-2}.$$

Figure 4: Leading particle and multiplicity cross sections. Displayed are the multiplicity cross sections and the leading pion and leading proton cross sections for the inelastic events.

TABLE I

Topological Cross Sections in 147 GeV/c $\pi^-$ p Interactions

| Number of Prongs | Events Found | Corrected Number | Cross Section (mb.) |
|---|---|---|---|
| 2 | 1276 | 1592 ± 52 | 5.15 ± 0.17 |
| | | Elastic 952 ± 64<br>Inelastic 640 ± 52 | Elastic 3.08 ± 0.21<br>Inelastic 2.07 ± 0.17 |
| 3 | 9 | | |
| 4 | 1194 | 1266 ± 40 | 4.10 ± 0.14 |
| 5 | 0 | | |
| 6 | 1351 | 1424 ± 40 | 4.61 ± 0.14 |
| 7 | 5 | | |
| 8 | 1299 | 1350 ± 38 | 4.37 ± 0.14 |
| 9 | 16 | | |
| 10 | 939 | 970 ± 33 | 3.14 ± 0.11 |
| 11 | 4 | | |
| 12 | 526 | 536 ± 25 | 1.74 ± 0.08 |
| 13 | 9 | | |
| 14 | 244 | 251 ± 17 | 0.81 ± 0.06 |
| 15 | 2 | | |
| 16 | 114 | 115 ± 11 | 0.37 ± 0.04 |
| 17 | 5 | | |
| 18 | 50 | 51 ± 7 | 0.17 ± 0.02 |
| 19 | 0 | | |
| 20 | 26 | 26 ± 5 | 0.084 ± 0.016 |
| 21 | 0 | | |
| 22 | 4 | 4 ± 2 | 0.013 ± 0.006 |
| 23 | 0 | | |
| 24 | 1 | 1 ± 1 | 0.003 ± 0.003 |
| Total | 7074 | 7586 ± 92 | 24.6 ± 0.4<br>3.1<br>21.5 |

TABLE II

Multiplicity Moments

| | 50 [a] | 100 [b] | 147 | 205 [c] |
|---|---|---|---|---|
| $\langle n \rangle$ | 5.78 ± 0.04 | 6.79 ± 0.08 | 7.34 ± 0.10 | 8.02 ± .12 |
| $\langle n(n-1) \rangle$ | 34.9 ± 0.48 | 49 ± 1 | 59.4 ± 1.1 | 71.6 ± 1.8 |
| $\langle n^2 \rangle$ | 40.7 ± 0.48 | 56 ± 1 | 66.7 ± 1.2 | 79.6 ± 1.8 |
| $f_2$ | 1.53 ± 0.15 | 3.2 ± 0.3 | 5.5 ± 0.5 | 7.24 ± 0.61 |
| D | 2.70 ± 0.03 | 3.16 ± 0.04 | 3.58 ± 0.05 | 3.91 ± 0.11 |
| $\langle n \rangle / D$ | 2.14 ± 0.03 | 2.15 ± 0.04 | 2.04 ± 0.04 | 2.05 ± 0.05 |

TABLE III

Leading Particle Cross Sections (mb.)

| | 2-prong (inelastic) | 4-prong | 6-prong |
|---|---|---|---|
| Leading pion | . 79 ± 0. 20 | . 91 ± 0. 16 | . 18 ± 0. 09 |
| Leading proton | . 66 ± 0. 11 | . 93 ± 0. 12 | . 40 ± 0. 13 |
| Leading pion + leading proton | 1. 45 ± 0. 23 | 1. 84 ± 0. 20 | . 58 ± 0. 16 |
| Total inelastic cross section | 2. 07 ± 0. 17 mb. | 4. 10 ± 0. 14 mb. | 4. 61 ± 0. 14 mb. |

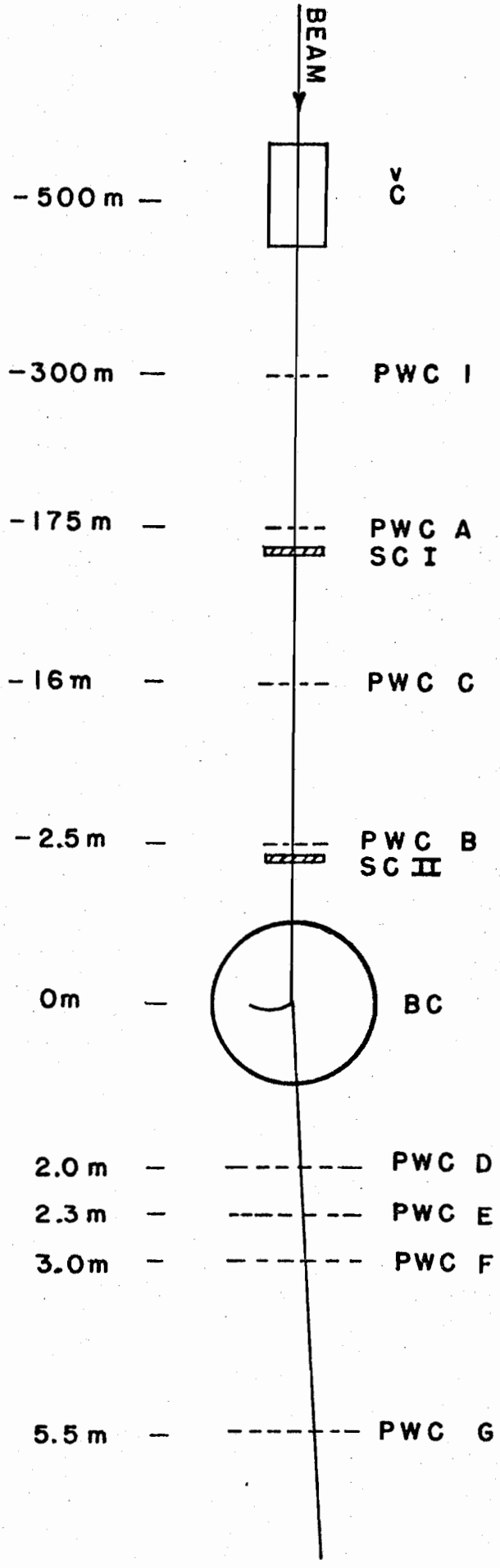
BEAM
-500 m
VC
-300 m
PWC I
-175 m
PWC A
SC I
-16 m
PWC C
-2.5 m
PWC B
SC II
0m
BC
2.0 m
PWC D
2.3 m
PWC E
3.0m
PWC F
5.5 m
PWC G

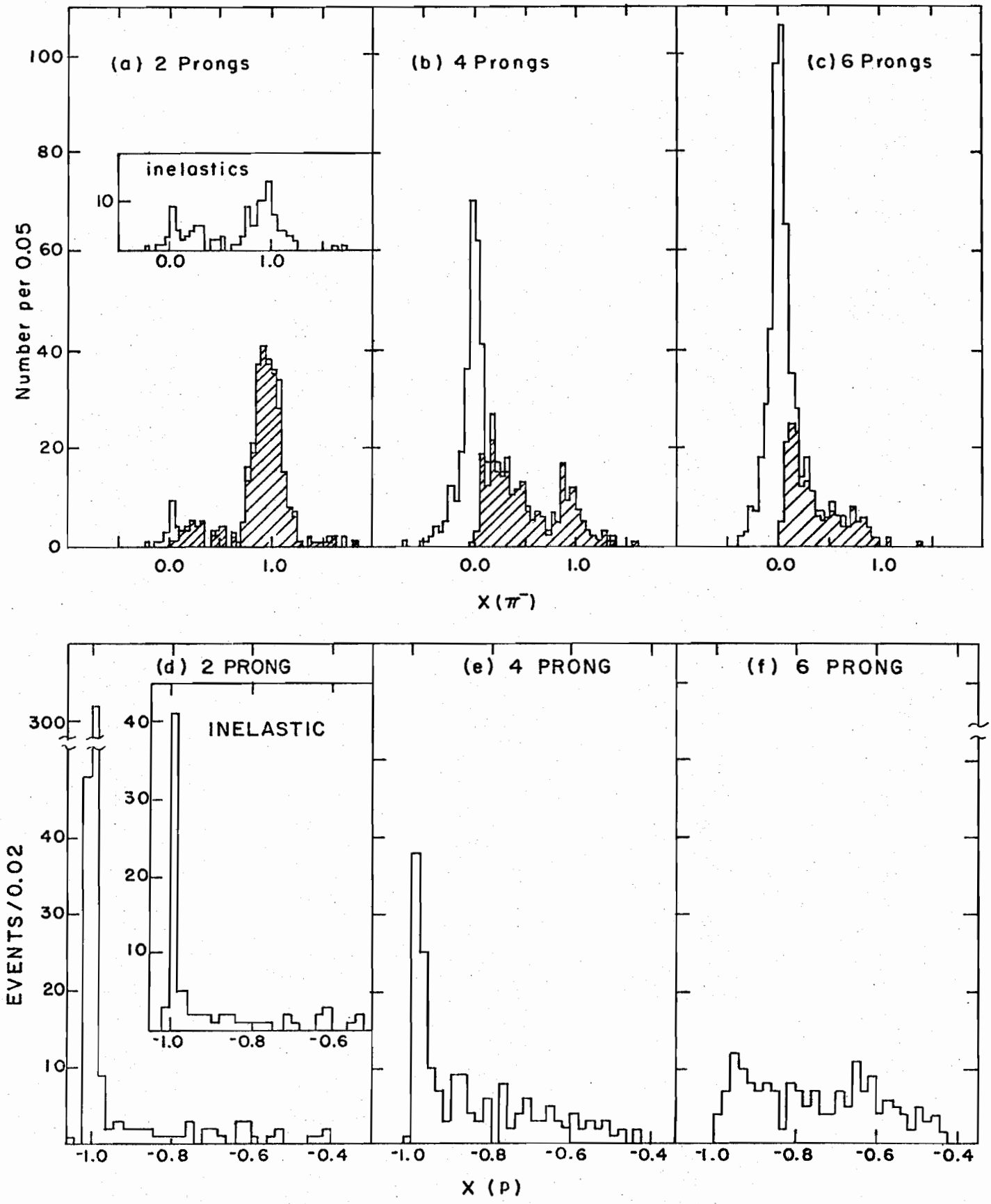
(a) 2 Prongs
(b) 4 Prongs
(c) 6 Prongs
inelastics
Number per 0.05
X (π⁻)
(d) 2 PRONG
(e) 4 PRONG
(f) 6 PRONG
INELASTIC
EVENTS/0.02
X (p)

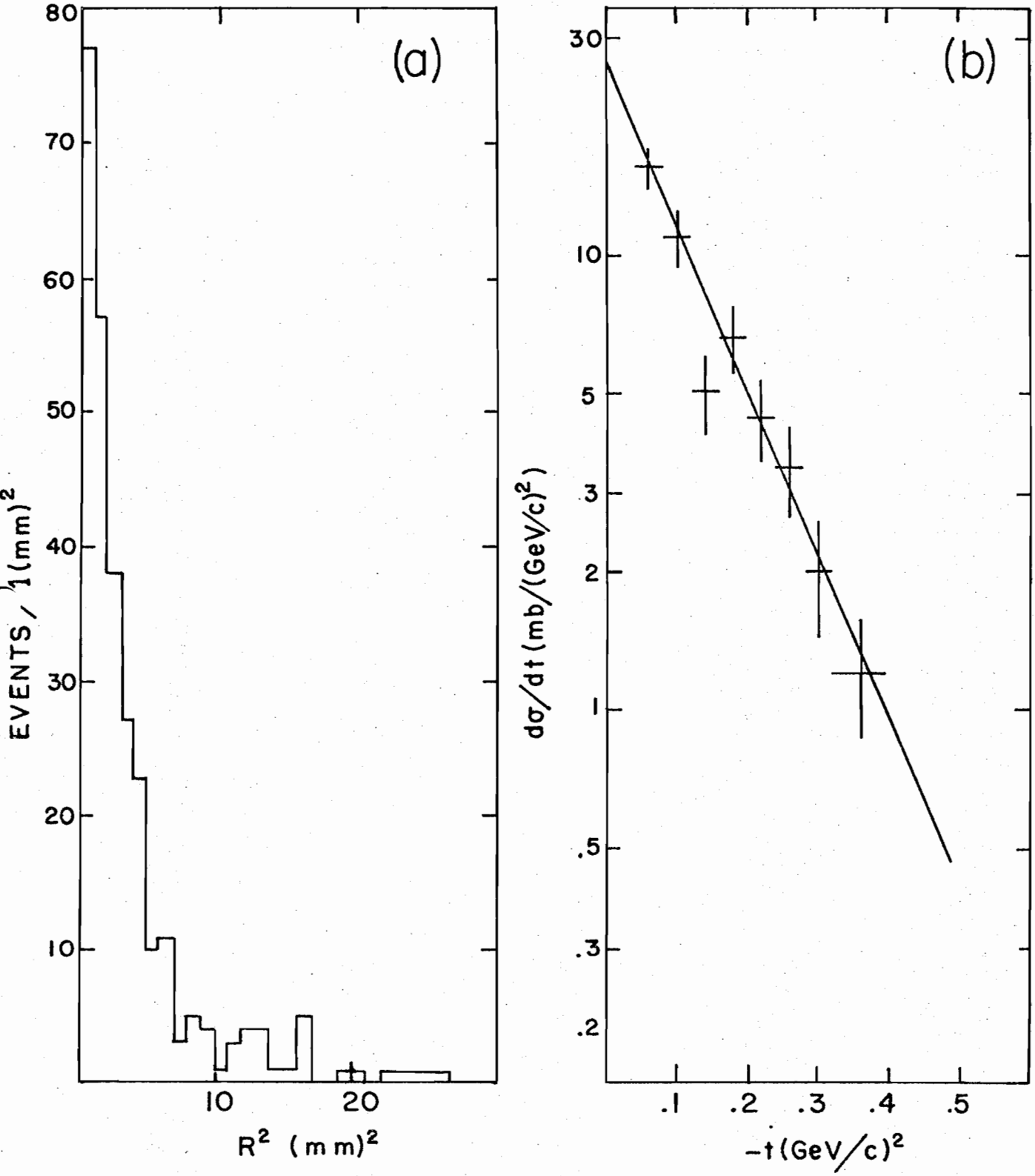
(a)
80
70
60
50
40
30
20
10
EVENTS / 1 (mm)²
10
20
R² (mm)²
(b)
30
10
5
3
2
1
.5
.3
.2
dσ/dt (mb/(GeV/c)²)
.1
.2
.3
.4
.5
-t (GeV/c)²

Charged Prong Multiplicities
Inelastic Events

- ● All charged
- ○ Leading pion
- × Leading proton
- △ Total leading particle